Characterization of crystalline and amorphous forms of irbesartan by multi-nuclear solid-state NMR

Marcin Skotnicki [a,*], Paul Hodgkinson [b,*]

[a] *Chair and Department of Pharmaceutical Technology, Poznan University of Medical Sciences, ul. Grunwaldzka 6, 60-780 Poznan, Poland*

[b] *Department of Chemistry, Durham University, South Road, Durham, DH1 3LE, United Kingdom*

[*]Corresponding authors:

Marcin Skotnicki, Chair and Department of Pharmaceutical Technology, Poznan University of Medical Sciences, ul. Grunwaldzka 6, 60-780 Poznan, Poland, E-mail: marcskot@ump.edu.pl

Paul Hodgkinson, Department of Chemistry, Durham University, South Road, Durham, DH1 3LE, UK. E-mail: paul.hodgkinson@durham.ac.uk

ABSTRACT

Irbesartan (IRB) is an antihypertensive drug which exhibits the rare phenomenon of desmotropy; its 1*H*- and 2*H*- tetrazole tautomers can be isolated as distinct crystalline forms. The crystalline forms of IRB are poorly soluble, hence the amorphous form is potentially of interest for its faster dissolution rate. The tautomeric form and the nature of hydrogen bonding in amorphous IRB are unknown. In this study, crystalline form A and amorphous form of irbesartan were studied using ^{13}C, ^{15}N and ^{1}H solid-state NMR. Variable-temperature ^{13}C SSMNR studies showed alkyl chain disorder in the crystalline form of IRB, which may explain the conflicting literature crystal structures of form A (the marketed form). ^{15}N NMR indicates that the amorphous material contains an approximately 2:1 ratio of 1*H*- and 2*H*-tetrazole tautomers. Static ^{1}H SSNMR and relaxation time measurements confirmed different molecular mobilities of the samples and provided molecular-level insight into the nature of the glass transition. SSNMR is shown to be a powerful technique to investigate the solid state of disordered active pharmaceutical ingredients.

Keywords: irbesartan, active pharmaceutical ingredient, amorphous form, solid-state NMR, tautomerism, desmotropy, molecular mobility, nitrogen-15 SSNMR, spin–lattice relaxation time

1 Introduction

Irbesartan (IRB, Figure 1) is a drug belonging to a family of angiotensin II type 1 (AT_1) receptor blockers known as sartans. It is indicated for the treatment of essential hypertension and diabetic nephropathy in hypertensive patients with type 2 diabetes [1].

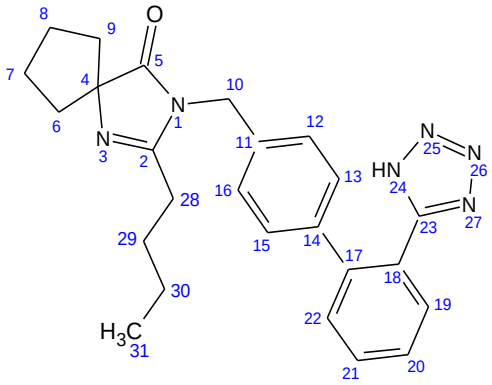

Figure 1. Chemical structure of irbesartan (2-butyl-3-[*p*-(*o*-1*H*-tetrazol-5-ylphenyl)benzyl]-1,3-diazaspiro[4.4]non-1-en-4-one) with carbons and nitrogens numbered according to the scheme used by Bauer *et al.* [2].

Most sartans contain a tetrazole ring in their structure, for instance, irbesartan, candesartan, valsartan, olmesartan and losartan [3], and so may exist as 1*H*- or 2*H*- tautomers, Figure 2. Due to the acidity of the tetrazole ring [4], sartans in biological systems exist largely as anions, hence the tautomeric state is not significant for their biological function [5]. However, the solid-state form of active pharmaceutical ingredient (API) can have a significant impact on the dissolution kinetics, especially for poorly soluble APIs, and thence on the overall bioavailability [6,7]. Irbesartan is such an example of a poorly soluble drug. Two crystalline (forms A and B) [2,8–14] and an amorphous form [15,16] of irbesartan are known. The crystal structure of form B is known [8] and has been deposited in Cambridge Structural Database (CSD), while conflicting structure solutions of form A are present in the literature [10], despite form A being the marketed form. Irbesartan is a rare example of a drug that exhibits desmotropes [17,18]. Its tautomers can be isolated in the solid state [19,20], with form A containing the 1*H*- tautomer of the tetrazole and form B the 2*H*- tautomer [2,8–14]. Desmotropes are distinct from crystal polymorphs, which involve different crystalline forms with exactly the same atomic skeleton [21]. Form A is more soluble (by a factor of four) and is thus preferred for formulation [10]. Araya-Sibaja *et al*. indicated that form A and B are both stable at ambient conditions, but structural and/or chemical instability was observed in form B at 40 °C and 98% relative humidity, whereas form A was stable at these conditions [10]. However, there were recalls of

IRB form A/hydrochlorothiazide fixed-dose combination (Avalide®), due to the presence of form B in the formulation that potentially compromised the bioavailability of the drug product [22].

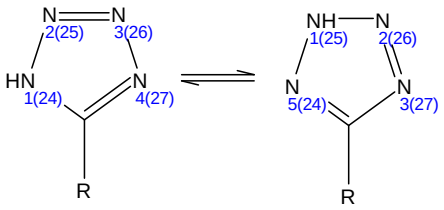

Figure 2. Possible tautomer of C-substituted tetrazole ring: (left) 1,2,3,4- (1*H*) tautomeric form, (right) 1,2,3,5- (2*H*) tautomeric form. In the brackets numbering used in this study for irbesartan is provided.

Tautomerisation is of paramount importance in the drug industry as there are a number of APIs [10,18,23–27] that may convert into another tautomer during the formulation process or in the final drug product, forming another polymorph, solvate or amorphous form [5,28–31] Thus, the API may exhibit different physicochemical properties, *i.e.*, solubility (irbesartan [10,22], albendazole [32]), stability during manufacturing process (ranitidine [33]) or hardness (omeprazole [34]). Tautomerisation is especially important in the case of an amorphous state. The amorphous state is of growing interest to pharmaceutical scientists due to better apparent solubility and bioavailability of these forms compared to their crystalline counterparts [35]. It is suggested that, by allowing different hydrogen-bond formation, tautomerisation of the API may help stabilise amorphous forms [30]. For example, the group of Paluch reported high physical stabilities (no tendency to crystallization) for amorphous forms of several APIs capable of tautomerization, e.g., glibenclamide [24], indapamide [25], and etoricoxib [26]. Thus, there is a need for strict quality control analysis of pharmaceutical raw materials in the solid-state with respect to tautomeric state. Moreover, if the tautomeric state is not established it is hard to understand hydrogen bonding and, thus the "structure" and stability of the amorphous material [26,36–38].

Solid-state NMR (SSNMR) spectroscopy is a non-destructive, powerful technique for obtaining structural and dynamic information on solid pharmaceutical systems [38–40] and is especially useful for characterizing amorphous solids [38,41,42] since standard Bragg diffraction techniques are of little value for materials lacking long-range order. NMR spectroscopy is the method of choice to study tautomerism [19,43], since it is directly sensitive to H locations. SSNMR has been used to characterise the solid state of forms A and B of irbesartan [2,11] as well as other sartans. The tautomeric form of known sartans investigated by single-crystal X-ray diffractometry and NMR is summarised in Table 1. These systems all

contain a (tetrazol-5-yl)biphenyl moiety and have confirmed biological activity. Note that some more recent sartans, such as eprosartan, do not contain this moiety and so are not considered here.

Table 1. Tautomeric forms of angiotensin II receptor antagonists (sartans).

Compound	Solid state form	Cambridge Structural Database identifier	Tautomeric form	Analytical method	Reference
Irbesartan	Crystalline form A	No agreed structure	1*H*	SSNMR	Bauer *et al.* .[2] Wang *et al.* [11] This study
	Crystalline form B	NOZWII	2*H*	SCXRD SSNMR	Böcskei *et al*. [8] Bauer *et al*. [2] Wang *et al.* [11]
	Amorphous		1*H*, 2*H* (ca. 2:1)	SSNMR	This study
Irbesartan bromide sesquihydrate	Crystalline	NIQVIT	1*H*	SCXRD	Wang *et al*. [44]
Irbesartan chloride hydrate	Crystalline	LIBZAY	1*H*	SCXRD	Bartolucci *et al*. [45]
Irbesartan 2,6-dihydroxybenzoate salt	Crystalline	YUQCEV	1*H*	SCXRD SSNMR	Wang *et al*. [11]
2-*n*-Butyl-1-((2'-(1*H*-tetrazol-5-yl)biphenyl-4-yl)methyl)-1*H*-benzimidazole-7-carboxylic acid methanol solvate	Crystalline	PELXAG10	1*H*	SCXRD	Kubo *et al.* [46]
	Crystalline	PELXAG	1*H*	SCXRD	Kubo *et al.* [47]
2-(*n*-Butyl)-6-methyl-5-(1-oxopyrid-2-yl)-1-((2'-(1*H*-tetrazol-5-yl)biphenyl-4-yl)methyl)-1*H*-imidazo(5,4-b)pyridine methanol solvate	Crystalline	HOFKUI	1*H*	SCXRD	Heo *et al*. [48]
2-*n*-Butyl-6-dimethoxymethyl-5-phenyl-1-((2'-(1*H*-tetrazol-5-yl)biphenyl-4-yl)methyl)-1*H*-imidazo(5,4-b)pyridine	Crystalline	ZUHTEB	1*H*	SCXRD	Shin *et al.* [49]
Candesartan cilexetil	Crystalline form I	FETWEH	1*H*	SSNMR SCXRD	Fernandez *et al.* [50] Matsunaga *et al*. [51]
	Crystalline form II	Not available	Not investigated	SSNMR	Matsunaga *et al*. [51]
	Amorphous		Not investigated	SSNMR	Matsunaga *et al*. [51]
Candesartan cilexetil acetone solvate	Crystalline	HIQTAF	1*H*	SCXRD	Gao *et al*. [52]
Ammonium candesartan-ide	Crystalline	GUNKEH	1*H*	SCXRD	Chi *et al.* [53]
2,7-Diethyl-6-hydroxymethyl-5-((2'-(1*H*-tetrazol-5-yl)biphenyl-4-yl)methyl)-5*H*-pyrazolo(1,5-b)(1,2,4)triazole	Crystalline	PUSNAS	1*H*	SCXRD	Okazaki *et al.* [54]
2,7-Diethyl-5-((2'-(1*H*-tetrazol-5-yl)biphenyl-4-yl)methyl)-5*H*-pyrazolo(1,5-b)(1,2,4)triazole	Crystalline	PUSMEV	1*H*	SCXRD	Okazaki *et al*. [55]
2-Ethyl-5,6,7,8-tetrahydro-4-((2'-(1*H*-tetrazol-5-yl)biphenyl-4-yl)methoxy)quinoline hydrochloride	Crystalline	SUKPET	1*H*	SCXRD	Bradbury *et al*. [56]
Ethyl 2-butyl-4-((3,3-dimethylacryloyl)methylamino)-1-((2'-(1*H*-tetrazol-5-yl)biphenyl-4-yl)methyl)-1H-imidazole-5-carboxylate	Crystalline	BIZRIL	1*H*	SCXRD	Okazaki *et al.* [57]
Ethyl 2-butyl-4-((3,3-dimethylacryloyl)amino)-1-((2'-(1*H*-tetrazol-5-yl)biphenyl-4-yl)methyl)-1*H*-imidazole-5-carboxylate methanol solvate	Crystalline	BIZROR	1*H*	SCXRD	Okazaki *et al.* [57]
3-((5-Hydroxy-4,4,6,6-tetramethyl-5,6-dihydro-4*H*-thieno[2,3-c]pyrrol-2-yl)methyl)-2,6-dimethyl-5-((2'-(1*H*-tetrazol-5-yl)biphenyl-4-yl)methyl)pyrimidin-4(3*H*)-one radical ethyl acetate solvate	Crystalline	UBULAG	1*H*	SCXRD	Tan *et al.* [58]
Losartan free acid	Crystalline	OCAHAC	2*H*	SCXRD	Tessler and Goldberg [59]
Losartan ethanol solvate (DuP 753 ethanol solvate)	Crystalline	Not available	1*H*	SCXRD	Okazaki *et al*. [55]
Olmesartan	Crystalline	ZOGSOD	1*H*	SCXRD	Yanagisawa *et al*. [60]
Olmesartan medoxomil	Crystalline	ZOGTAQ02	1*H*	SCXRD	Betz *et al*. [61]
PNU-97018	Crystalline	HUNWES	2*H*	SCXRD	Ishii *et al.* [62]
PNU-97018 methanol solvate	Crystalline	HUNWIW	1*H*	SCXRD	Ishii *et al.* [62]
PNU-97018 ethanol solvate	Crystalline	HUNWOC	1*H*	SCXRD	Ishii *et al.* [62]
2-propyl-1-((2'-(1*H*-tetrazol-5-yl)biphenyl-4-yl)methyl)-1,2-dihydro-3*H*-pyrazolo[3,4-b]pyridin-3-one	Crystalline	VOKFEI	1*H*	SCXRD	Cappelli *et al*. [63]
Tasosartan (ANA-756)	Crystalline	WELGAV	1*H*	SCXRD	Ellingboe *et al.* [64]
Valsartan	Crystalline	KIPLIG	1*H*	SCXRD	Wang *et al*. [65]
	Amorphous with some degree of order			SSNMR	Skotnicki *et al.* [66]

	Fully amorphous				
Valsartan ethanol solvate	Crystalline	KIPLEC	1*H*	SCXRD	Wang *et al*. [65]

In this study, crystalline form A and the amorphous form of irbesartan were characterised to provide insight into the tautomeric form and molecular mobility by employing ^{13}C, ^{15}N, ^{1}H MAS and ^{1}H static SSNMR.

2 Material and methods

2.1 Materials

Irbesartan (crystalline form A; pharmaceutical grade) was obtained from Polpharma, Starogard Gdański, Poland and used without further treatment. Its amorphous form (form AM) was prepared immediately prior to experimental measurements by heating the sample in an oven to 186 °C, holding for 10 min then cooling with at least approximately 5 °C min^{-1} cooling rate to room temperature.

2.2 Solid-state NMR measurements

Carbon-13 solid-state NMR spectra were acquired using a Varian InfinityPlus spectrometer operating at a ^{13}C frequency of 125.68 MHz. A magic-angle spinning (MAS) probe using 5 mm diameter zirconia rotors was employed. Typical operating conditions used cross-polarisation (CP) for excitation of the ^{13}C magnetization, with a CP contact time of 1 or 3 ms (amorphous and crystalline respectively), a recycle delay of 4 s, 512 transients and spin rate of 10 kHz. SPINAL-64 sequence for ^{1}H decoupling was applied during signal acquisition [67]. Carbon chemical shifts were referenced to the signal for tetramethylsilane *via* a replacement sample of solid adamantane (38.4 ppm for the high-frequency line). Variable-temperature experiments were performed from 38 °C to 140 °C, allowing samples to stabilize for 15–20 min before starting acquisition. Unless otherwise stated, temperatures in these experiments are quoted with a correction of +16 °C above the displayed temperature, which is the estimated increase in sample temperature for a 5 mm rotor spinning at 10 kHz, based on previous calibration experiments using lead nitrate [68].

Proton MAS spectra were recorded using the same spectrometer operating at a ^{1}H frequency of 499.70 MHz, and a Bruker MAS probe using 1.3 mm diameter zirconia rotors. Spectra were typically acquired using a recycle delay of 10 s, 64 transients and spin rate of 67 kHz. Spectra were also recorded at 43 and 53 kHz spinning rate, where frictional heating is significantly lower, and gave identical results apart from lower spectral resolution. Proton broadline NMR spectra and proton relaxation times (T_1^{H} and $T_{1\rho}^{H}$) for static samples were measured at 299.82

MHz using a Varian UnityPlus spectrometer. T_1^H was measured using saturation-recovery experiments [69]. For $T_{1\rho}^H$ spin-locking, a radio frequency field equivalent to 70 kHz was used. Spectra were measured over a temperature range from 25 to 120 °C, allowing at least 15 min for stabilization before the acquisition. Uncertainties listed are the standard errors in the parameters as determined from non-linear regression analysis using SigmaPlot 12.0 (Systat Software Inc., San Jose, CA, USA).

Nitrogen-15 solid-state NMR spectra were recorded with CP and MAS using the Varian InfinityPlus spectrometer, operating at ^{15}N frequency of 50.65 MHz, and a probe taking 5 mm diameter rotors. Typical operating conditions used a CP contact time of 10 or 20 ms, a recycle delay of 4 or 5 s, 11 000 to 86 0000 transients and spin rate of 10 kHz. Nitrogen chemical shifts were referenced using ^{15}N-enriched glycine at –347.4 ppm relative to the signal of neat nitromethane. Inversion-recovery (IR) CP MAS experiments were recorded with an inversion time of 1 and 2 ms as described in Ref. [70]. The spectrum for the amorphous sample was smoothed using 3rd degree polynomial with 25 points using ACD/Spectrus Processor.

Data were processed using Gsim software [71] or ACD/Spectrus Processor v. 2021.1.2 (Advanced Chemistry Development Inc., Toronto, Canada).

3 Results and discussion

3.1 Carbon-13 SSNMR

Figure 3 shows ^{13}C CP MAS NMR spectra of the crystalline (form A) and amorphous irbesartan forms. The spectra for both forms are quite distinct, reflecting substantial differences in the structure between two solid forms. The spectrum of amorphous form is also significantly different than that of crystalline form B [2]. As expected, the resonances of amorphous irbesartan are significantly broader, reflecting of the distribution of local environments and hence a dispersion of chemical shifts in the disordered material. Table S1 (Supplementary material) lists the chemical shifts for crystalline (forms A and B) and amorphous solid forms of irbesartan. The resonances were assigned based on previous reports for irbesartan form A and B [2]. The most significant difference between crystalline and amorphous forms is for the methyl resonances (C-31). A low intensity signal associated with C-31 can be observed in previously published spectra for form A, but was not discussed [2,11]. In the amorphous material, the signal that arises from C-31 is broadened and moves to a higher chemical shift of 14.0 ppm ($\Delta\delta$ = –2.2 ppm) in comparison to crystalline form A. The shift of C-31 signal in the

amorphous form may indicate that amorphous form contains 2*H*- tautomer as it is similar to form B (2*H*-), *i.e.*, 15.4 ppm [2,11].

The signals between 120 and 150 ppm arise from the phenyl rings. The remaining signals come from the carbon in the tetrazole ring (C-23), imidazolinone ring (C-2) and carbonyl group (C-5) respectively. The imidazolinone ring carbon (C-2) and the carbon in the tetrazole ring (C-23) are difficult to unambiguously assign in the amorphous form as there are three resonances in this region at 166.2, 161.5 and 154.9 ppm. The most plausible explanation for this increase in signals is the presence of both tautomers. In particular, the additional signal at 161.5 ppm is most likely to arise from C-23 in the 2*H*- tautomer – this peak appears at 164.9 ppm in form B [2,8,11].

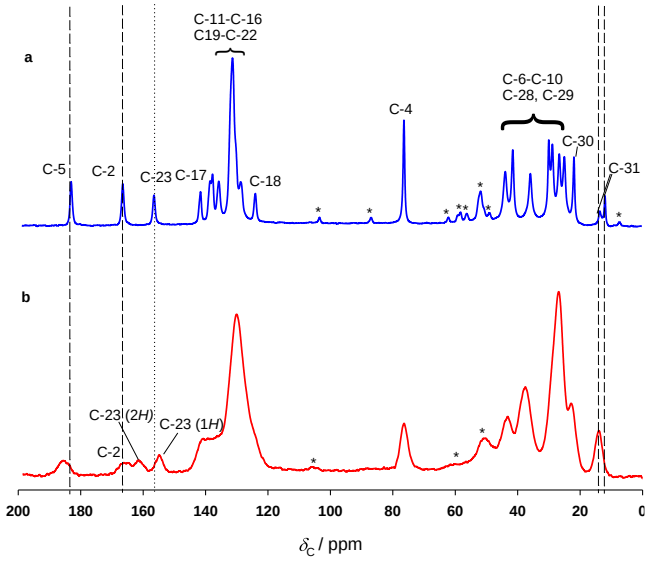

Figure 3. Carbon-13 CP MAS NMR spectra of (a) crystalline (form A) and (b) amorphous irbesartan. Spectra recorded at 10 kHz spinning rate at 38 °C.

To investigate differences in mobility, carbon-13 CP MAS variable temperature (VT) SSNMR spectra were acquired (Figure 4; see Figure S1 in the Supplementary material for all investigated temperatures). The spectra of crystalline material did not change significantly, except for the methyl resonance. At 140 °C, the previously low-intensity signal from methyl (C-31) at 13.4 ppm and the signal at 11.8 ppm have approximately equal intensity. The changes in the methyl resonance are unlikely to be due to interaction between methyl diffusional rotation and ^{1}H decoupling, since such effects only occur at temperatures of about 100 K and below [72]. A more plausible explanation is the presence of disorder in the alkyl chain, which may exist in two overall conformations which are equally occupied at higher temperature. A non-quaternary suppression experiment, Figure S2 (Supplementary material), confirms that two of

the methylene units of the butyl chain are unusually mobile (such experiments typically supress CH_2 resonances very effectively). Similar behaviour has been observed in the ^{13}C spectrum of losartan potassium [73], which was also ascribed to disorder of the *n*-butyl chain. Disorder in the *n*-butyl chain was also found by SCXRD for form B of IRB [8]. This disorder may explain why there is no definitive literature structure for form A [10], since the presence of a minority conformation will severely complicate the modelling of diffraction data. In the spectra of the amorphous material, there is a noticeable reduction in the methyl (C-31), methylene (C-30) and carbon in the imidazolinone ring (C-4) peak linewidth at 140 °C. As discussed further below, this change occurs significantly above the glass transition at 76 °C [74]. In contrast, the aromatic region material above the glass transition has significantly broadened. This broadening is typical of interference of between molecular motion and the RF nutation frequency during ^1H decoupling, which is of the order of 50 kHz. This combination of line-narrowing of the alkyl region and line-broadening of the aromatic regions implies fast motions of alkyl group and slower large scale motions involving the aromatic core. This large scale motion is only present well above T_g. This behaviour is consistent with the relaxation time data as described below.

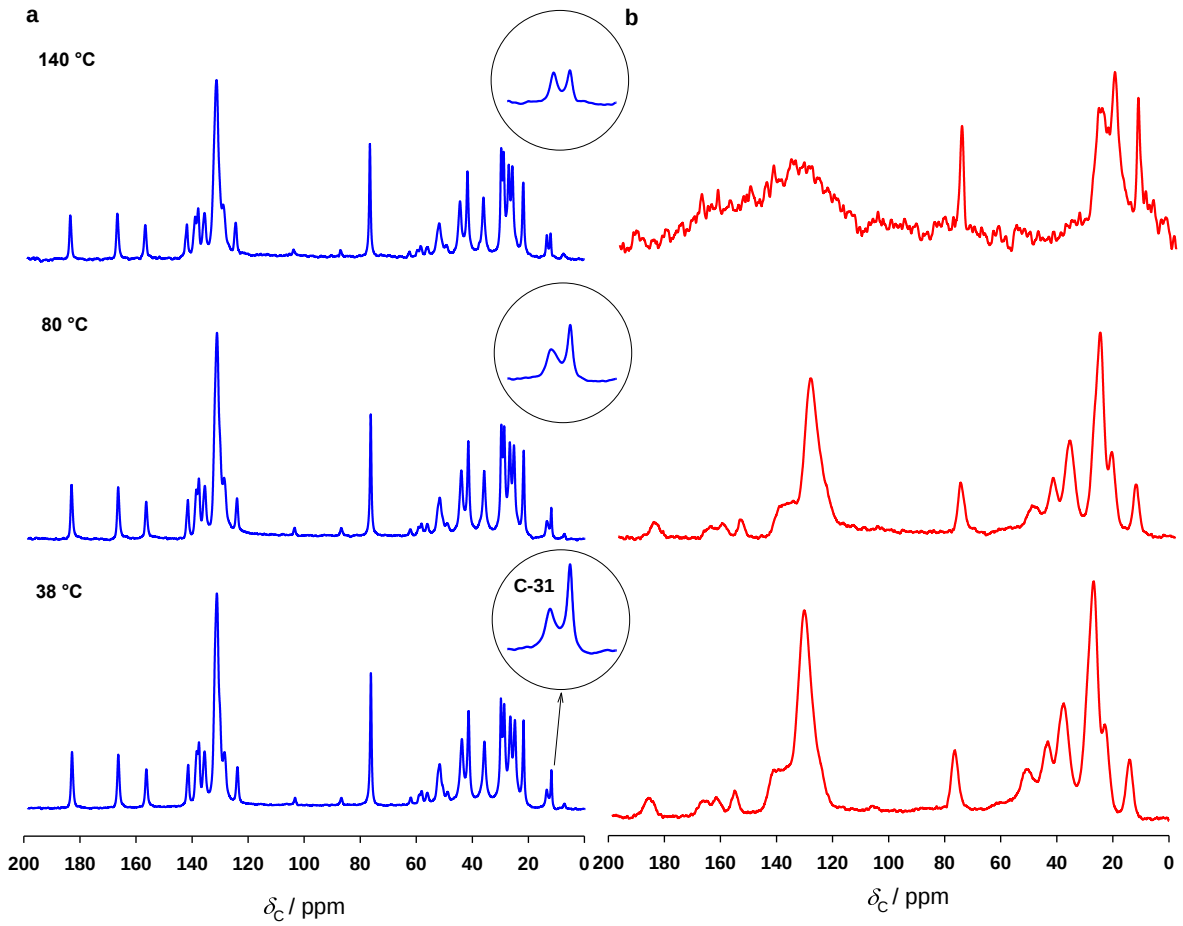

Figure 4. Variable-temperature ^{13}C CP MAS spectra of (a) form A and (b) the amorphous form irbesartan. 512 scans were acquired except for the spectrum of amorphous form at 140 °C where 1024 scans were acquired (and also a line broadening of 100 Hz was applied). The spectra of crystalline material did not change significantly, except for signals arising from methyl (C-31).

3.2 Nitrogen-15 SSNMR

Nitrogen-15 NMR spectroscopy is widely used in studies of nitrogen-containing molecules and tautomerism both in solution- and solid- state [43,75,76]. Due to its low natural abundance (0.37%) and poor relative receptivity (3.84×10^{-6}) [69], these studies are time-consuming and not always feasible, especially for amorphous materials [77] (although dynamic nuclear polarization techniques show promise in overcoming these limitations [77–79]).

Figure 5 shows ^{15}N CP MAS NMR spectra of both irbesartan forms. The crystalline material gives 6 clear signals, as expected. The assignment was confirmed by spectral editing experiments and was compared to previously published data for form A and B [2], cf. Table 2. The signal at –216.7 ppm can be easily assigned to N-1. As previously observed on a related system [66], standard dipolar dephasing experiments were not effective in identifying the protonated nitrogen, thus the inversion-recovery (IR) CP MAS technique was employed [70].

This confirmed that signal at –143.9 ppm arises from N-24, *i.e.*, the protonated nitrogen, Figure 5a and c. Furthermore, it can be observed that the signal at −139.1 ppm (N-3) is negative with a longer inversion contact time, suggesting that this nitrogen is involved in hydrogen bonding, Figure 5c. The spectrum of the amorphous form (Figure 5d) shows 9 poorly resolved signals. The amorphous nature of the material and low ^{15}N natural abundance limits the signal-to-noise ratio of the spectrum. However, two partly resolved signals for N-1 (−218.9, −228.5 ppm) are observed. The spectra of crystalline forms show signals for N-1 at −216.7 and −219.0 ppm for desmotrope A and B respectively[2], hence the two signals of N-1 in the amorphous material suggest that it contains both 1*H*- and 2*H*- tautomers. This result is consistent with ^{13}C spectrum, where an additional signal, thought to be due to the tetrazole carbon (C-23), appeared. The N-3 and tetrazole nitrogens could not be unambiguously assigned. The chemical shifts are significantly different to those of the starting crystalline material form A (except N-26 and N-27), and form B (except N-27) and there is an extra resonance at −108.0 and −113.3 ppm. IR CP MAS experiments to identify protonated sites were not feasible due to poor sensitivity. A suggested assignment is shown in Figure 5d. The signals from 1*H*- tautomer are assumed to be at similar frequencies, but broadened, compared to crystalline form A. The signals for 2*H*-tautomer are more difficult to unambiguously assign. The signals at –108.0 and −113.3 ppm arise most likely from N-24 and N-25 of 2*H*- tautomer. The spectrum, however, is clearly consistent with a mix of tautomers. Note that the signals from the tetrazole ring in Form B (2*H*-tautomer) were broadened by dynamics at ambient temperature in the original study (hence the lower observation temperature), but such effects are not apparent in the ^{15}N spectrum of the amorphous material.

Table 2. Nitrogen-15 CP MAS NMR chemical shifts for crystalline (form A) and amorphous irbesartan recorded at 10 kHz spinning rate at 38 °C, compared to previously reported data for form A and B [2].

Solid state	**Tautomeric form**	**N-1**	**N-3**	**N-24**	**N-27**	**N-25**	**N-26**
Form A (this work)	1*H*	−216.7	−139.1	−143.9	−54.3	−13.8	12.7
Form A (ref. [2]**)**	1*H*	−216.4[a]	−140.2[a]	−143.6	−54.6	−13.3	13.4
Form B (ref. [2]**)**[b]	2*H*	−219.0[a]	−143.9[a]	−79.3	−50.7	−88.7	−3.2
Amorphous form (this work)	1*H*, 2*H* (ca. 2:1)	−218.9, −228.5	−145.1, −136.9, −113.3, −108.0, −50.1, −13.5				17.9

[a]the chemical shifts originally reported as referenced to NO_3^- signal of solid NH_4NO_3

[b]acquired at −20 °C

In the amorphous phase, the 1*H*-tautomer predominates (ca. 2:1, based on the N-1 resonance). Generally, the reported research on tetrazole-containing molecules shows that one tautomer is present in the crystalline form [2,8,59,62,80–86]. Both forms are present in solution [2], and the ratio strongly depends on the electrophilicity of substituent and polarity of the solvent [87]. In the gas phase, the 2*H*-form predominates [74,88–90]. Araya-Sibaya *et al*. argued that the formation of crystalline form B of irbesartan (2*H*-tautomer) from the solution is driven by high polarity and high polarizability of the solvent [91], although this seemingly conflicts with the conclusion of Butler *et al.*[87] that less polar solvents orient the tautomerism towards 2*H*-tautomer.

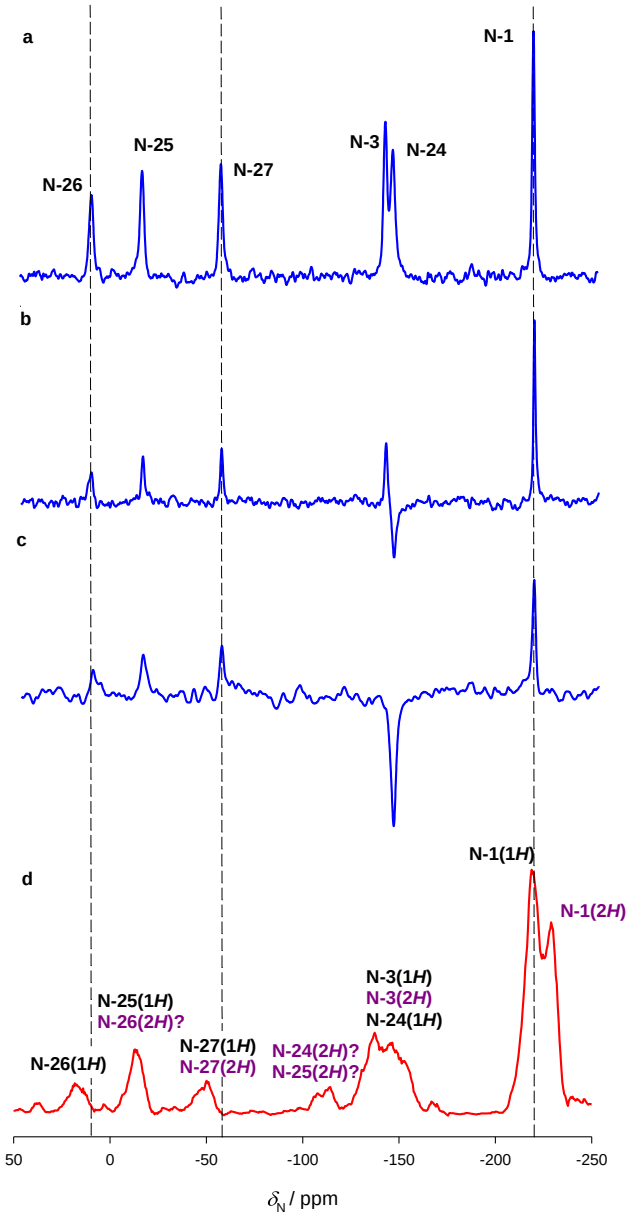

Figure 5. Nitrogen-15 CP MAS spectra of (a) irbesartan form A (11 000 repetitions, contact time (CT) of 20 ms) (b) ^{15}N IR CP MAS spectrum of form A (15 000 repetitions, CT = 10 ms and inversion time (IT) = 1 ms) (c) as

(b) but with IT = 2 ms (and 18 000 repetitions) and (d) ^{15}N CP MAS spectrum of amorphous irbesartan (86 000 repetitions, CT = 10 ms).

3.3 Proton MAS SSNMR

As shown in Figure 6, four regions are clearly distinguished in the ^{1}H fast MAS spectrum of crystalline irbesartan: alkyls protons (0–4.4 ppm), protons from C-10 bonded to nitrogen in the imidazolinone ring (4.95 ppm), aromatic (5.6–10 ppm) and tetrazole (17.76 ppm) protons (see Table S2 of Supplementary material for detailed chemical shifts). The assignment of the signals was based on the previous proton solution-state NMR data [2]. As would be expected, only broad features are resolved for the amorphous form. The ^{1}H MAS experiment shows a very clear signal from tetrazole proton at high chemical shift, which implies strong hydrogen bonding in crystalline form A. In contrast, the ^{1}H spectrum of the fully amorphous form shows a very broad feature in this region, suggesting a much wider distribution of hydrogen bonding environments in the amorphous form. Similar behaviour was observed in the case of valsartan [66].

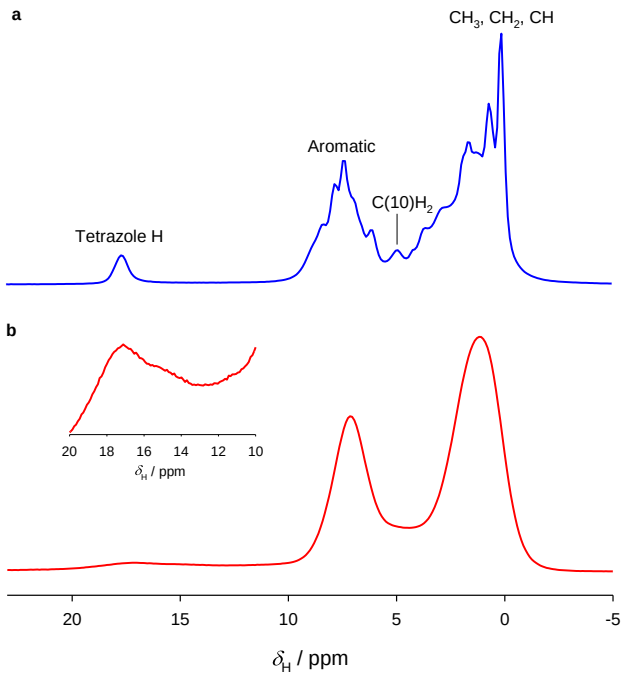

Figure 6. Proton MAS NMR spectra of (a) crystalline and (b) amorphous irbesartan recorded at a MAS rate of 67 kHz. Inset shows a magnification of the tetrazole proton region for amorphous form.

3.4 Static proton SSNMR

Figure 7 shows static ^{1}H variable-temperature (VT) SSNMR spectra of crystalline and amorphous irbesartan forms. As would be expected, these are broad and featureless due to

extensive ^{1}H, ^{1}H dipolar coupling. As the temperature increases from 25 to 120 °C, there are very small changes in the bandshapes for crystalline irbesartan. However, narrowing occurs for amorphous irbesartan at the temperature above 100 °C, consistent with an increase in mobility above the glass transition. As previously observed in the ^{13}C VT spectrum, however, the changes are very small at T_g (76 °C), and significant motional averaging is only observed above 100 °C.

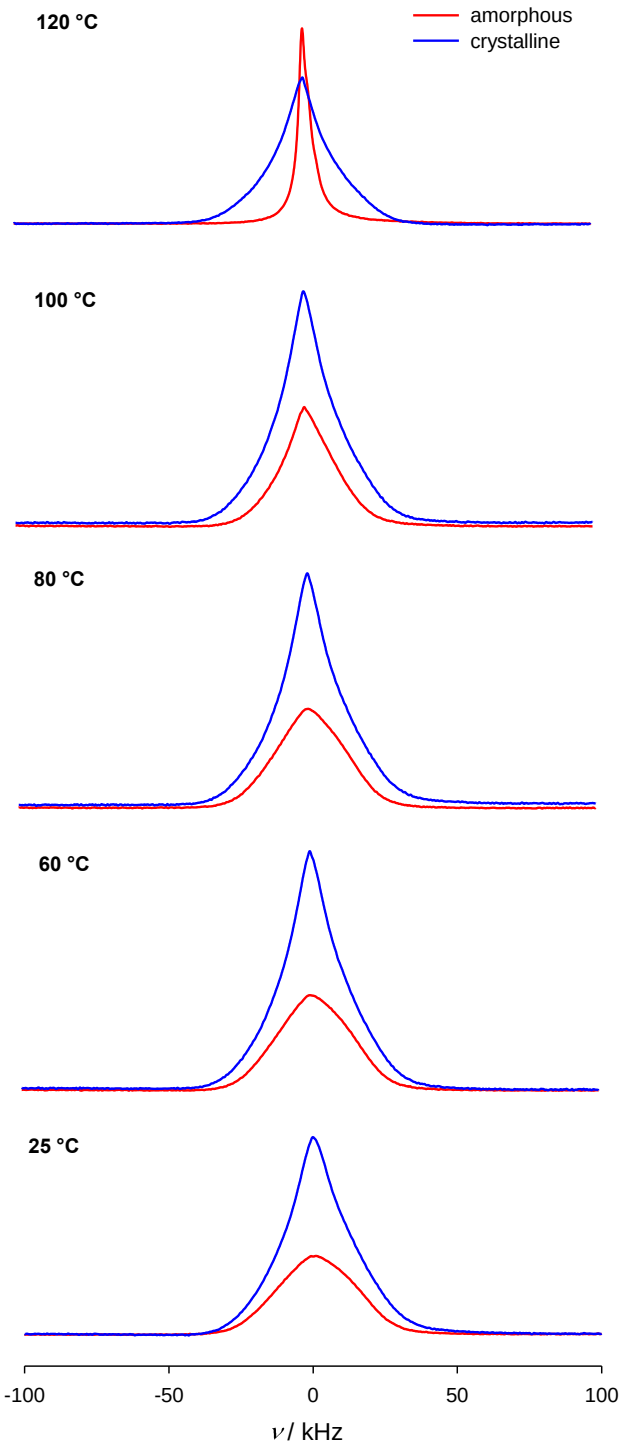

Figure 7. Variable-temperature static ^{1}H NMR spectra of crystalline (form A, blue line) and amorphous (red line) forms of irbesartan. The sharpening of bandshapes is observed with the increase of temperature for amorphous form and is only observed significantly above the glass transition temperatures (T_g = 76 °C).

Figure 8 shows ^{1}H spin–lattice relaxation time (T_1^H) as a function of temperature obtained for the examined irbesartan forms (data contained in Table S3 in Supplementary material). The T_1 relaxation time is sensitive to motion processes of the order of ^{1}H NMR frequency [92], here 400 MHz, and are likely to dominated by flexible groups, such as the butyl. The T_1^H

measurements show a monotonic increase in the T_1 values with increasing temperature for both forms, consistent with fast motions that exceed 400 MHz even at the lowest temperature. The values of T_1^H at room temperature are significantly different for both forms, consistent with faster (less hindered) dynamics in the amorphous material. The T_1^H values converge at the glass transition temperature (T_g = 76 °C) of the amorphous, implying that these rapid motions (e.g., alkyl motion) are similar at higher temperatures. This is consistent with the idea that the butyl group in form A is relatively unrestricted at higher temperatures, but this disorder is at least partially hindered at ambient temperature, leading to the unusual C-31 signal.

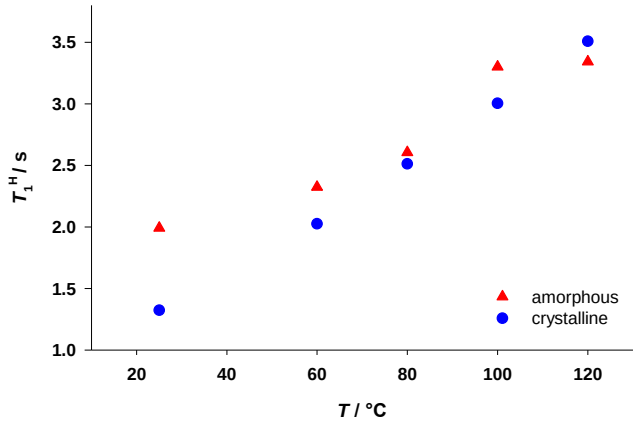

Figure 8. Proton spin–lattice relaxation time (T_1^H) for crystalline and amorphous irbesartan forms. The error bars are not shown as they are of a similar magnitude to the size of the symbols used.

The $T_{1\rho}$ relaxation behaviour is sensitive to motional processes of the order 70 kHz [92]. The $T_{1\rho}^H$ relaxation decays of the amorphous material are monoexponential, but the curves for the crystalline form are clearly biexpontential, containing two components with time constants of about 15 ms and about 160 ms (see Table S4 in Supplementary material for the data). "Spin diffusion" between ^{1}H nuclei means that the components in multi-exponential fitting have limited physical significance, and so Figure 9 plots the data from the crystalline form in terms of a single effective $T_{1\rho(\mathrm{eff})}^H$, calculated as reciprocal population weighted rate average (PWRA):

$$\frac{1}{T_{1\rho(\mathrm{eff})}^H} = \frac{A_{\mathrm{fast}}}{T_{1\rho(\mathrm{fast})}^H} + \frac{A_{\mathrm{slow}}}{T_{1\rho(\mathrm{slow})}^H} \qquad (1)$$

where A_{fast} and A_{slow} are the weighting fractions of the two components. The $T_{1\rho}^H$ of the amorphous material starts becoming shorter above T_g, indicating that at 120 °C the dynamics is approaching 70 kHz. These results are consistent with the phenomena observed in the ^{13}C spectra of Figure 4. The $T_{1\rho}^H$ values are generally shorter in the amorphous form, consistent with a greater overall amplitude of low frequency dynamics in a non-crystalline material. The amplitude / frequency of the dynamics monotonically increases with temperature until $T_{1\rho}^H$ is

very short, consistent with the line-broadening in the aromatic region of the ^{13}C spectrum. The midpoint of this evolution is close to the observed glass transition temperature. The short $T_{1\rho(\mathrm{eff})}^{\mathrm{H}}$ of the crystalline material at low temperature must have a different origin. The biexponential nature of the relaxation suggests that this is associated with a small part of the structure with distinctly different dynamics. This would be consistent with jumps of the conformationally disordered butyl chain. This behaviour is apparently not observed in the amorphous form, most likely because there are no trapped conformations in the amorphous material (the C-31 signal is unremarkable in the amorphous form).

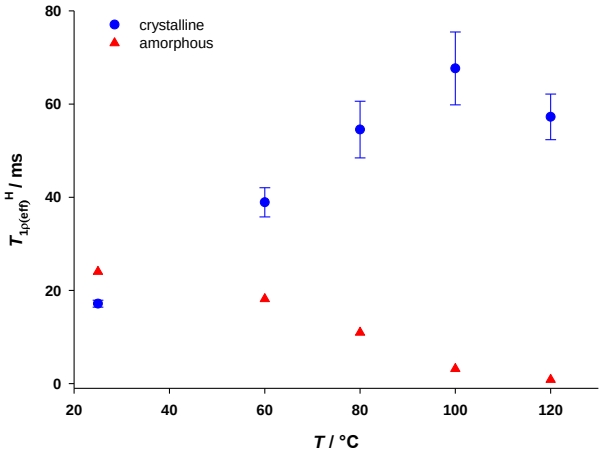

Figure 9. Static proton spin–lattice relaxation time in the rotating frame for crystalline and amorphous irbesartan forms. The error bars for amorphous form are not shown as they are of a similar magnitude to the size of the symbols used.

4 Conclusions

In conclusion, the tautomeric state and mobility of crystalline form A and amorphous form of irbesartan were investigated by multi-nuclear SSNMR. ^{13}C, ^{15}N and ultra-fast ^{1}H MAS experiments suggest that the amorphous material exists as a mixture of two tautomeric forms, with the 1*H*-tautomer predominating. The tautomerisation ability of irbesartan in the amorphous state may be responsible for its good physical stability [15,16], as this may provide additional flexibility for accommodating different hydrogen bonding arrangements [26].

^{13}C and ^{1}H NMR experiments also provided molecular level insight into disorder and dynamics in these materials. In particular the *n*-butyl chain appears to be trapped in two slowly exchanging conformations in form A, which may explain the difficulties in solving its crystal structure. This behaviour is not observed in the amorphous material. ^{1}H $T_{1\rho}$ relaxation times show the gradual onset of low-frequency dynamics either side of the glass transition temperature. This is consistent with T_g involving unlocking of the aromatic cores, although it is

important to note that large amplitude motions, leading to significant narrowing of the ^{1}H NMR spectrum, are only observed well above T_g.

Overall solid-state NMR is seen to provide detailed molecular-level insight into local protonation states and molecular mobility, even in highly disordered APIs, which are difficult to characterise by conventional approaches.

Declaration of competing interest

The authors declare that they have no known competing financial interests or personal relationships that could have appeared to influence the work reported in this paper**.**

Acknowledgments

The authors would like to thank Dr David C. Apperley from the Solid-State NMR Service at Durham for acquiring the static proton NMR spectra and Jamie L. Guest for reviewing a draft of the manuscript and acquiring the NQS experiment shown in the Supplementary material. The authors also acknowledge Polpharma SA Company (Starogard Gdański, Poland) for supplying irbesartan used in this study.

Appendix A. Supplementary material

Supplementary data to this article can be found online at:

References

1. Bramlage, P.; Durand-Zaleski, I.; Desai, N.; Pirk, O.; Hacker, C. The value of irbesartan in the management of hypertension. *Expert Opin. Pharmacother.* **2009**, *10*, 1817–1831, doi:10.1517/14656560903103820.

2. Bauer, M.; Harris, R.K.; Rao, R.C.; Apperley, D.C.; Rodger, C.A. NMR study of desmotropy in Irbesartan, a tetrazole-containing pharmaceutical compound. *J. Chem. Soc. Perkin Trans. 2* **1998**, 475–481, doi:10.1039/a708038g.

3. K. Vyas, V.; Ghate, M. Substituted Benzimidazole Derivatives as Angiotensin II -AT_1 Receptor Antagonist: A Review. *Mini-Reviews Med. Chem.* **2010**, *10*, 1366–1384, doi:10.2174/138955710793564151.

4. Myznikov, L. V.; Hrabalek, A.; Koldobskii, G.I. Drugs in the tetrazole series. (Review). *Chem. Heterocycl. Compd.* **2007**, *43*, 1–9, doi:10.1007/s10593-007-0001-5.

5. Katritzky, A.R.; Hall, C.D.; El-Gendy, B.E.-D.M.; Draghici, B. Tautomerism in drug discovery. *J. Comput. Aided. Mol. Des.* **2010**, *24*, 475–484, doi:10.1007/s10822-010-9359-z.

6. Censi, R.; Di Martino, P. Polymorph Impact on the Bioavailability and Stability of Poorly Soluble Drugs. *Molecules* **2015**, *20*, 18759–18776, doi:10.3390/molecules201018759.

7. Kothari, K.; Suryanarayanan, R. Influence of Disorder on Dissolution. In *Disordered Pharmaceutical Materials*; Descamps, M., Ed.; Wiley Online Books; Wiley Online Library,

2016; pp. 57–84 ISBN 9783527652693.

8. Böcskei, Z.; Simon, K. mán; Rao, R.; Caron, A.; Rodger, C.A.; Bauer, M. Irbesartan crystal form B. *Acta Crystallogr. Sect. C Cryst. Struct. Commun.* **1998**, *54*, 808–810, doi:10.1107/S0108270197019884.

9. Garcia, E.; Hoff, C.; Veesler, S. Dissolution and phase transition of pharmaceutical compounds. *J. Cryst. Growth* **2002**, *237–239*, 2233–2239, doi:10.1016/S0022-0248(01)02282-5.

10. Araya-Sibaja, A.M.; Maduro de Campos, C.E.; Fandaruff, C.; Vega-Baudrit, J.R.; Guillén-Girón, T.; Navarro-Hoyos, M.; Cuffini, S.L. Irbesartan desmotropes: Solid-state characterization, thermodynamic study and dissolution properties. *J. Pharm. Anal.* **2019**, *9*, 339–346, doi:10.1016/j.jpha.2019.07.001.

11. Wang, X.; Gao, D.; Li, D.; Xie, Q.; Deng, Z.; Zhang, H. Collecting the molecular and ionization states of Irbesartan in the solid state. *Cryst. Growth Des.* **2020**, *20*, 5664–5669, doi:10.1021/acs.cgd.0c00891.

12. Delaney, S.P.; Pan, D.; Galella, M.; Yin, S.X.; Korter, T.M. Understanding the origins of conformational disorder in the crystalline polymorphs of irbesartan. *Cryst. Growth Des.* **2012**, *12*, 5017–5024, doi:10.1021/cg300977e.

13. Veesler, S.; Lafferrère, L.; Garcia, E.; Hoff, C. Phase Transitions in Supersaturated Drug Solution. *Org. Process Res. Dev.* **2003**, *7*, 983–989, doi:10.1021/op034089f.

14. Garcia, E.; Veesler, S.; Boistelle, R.; Hoff, C. Crystallization and dissolution of pharmaceutical compounds an experimental approach. *J. Cryst. Growth* **1999**, *198–199*, 1360–1364, doi:10.1016/S0022-0248(98)01023-9.

15. Moura Ramos, J.J.; Diogo, H.P. Thermal behavior and molecular mobility in the glassy state of three anti-hypertensive pharmaceutical ingredients. *RSC Adv.* **2017**, *7*, 10831–10840, doi:10.1039/c7ra00298j.

16. Chawla, G.; Bansal, A.K. Molecular mobility and physical stability of amorphous irbesartan. *Sci. Pharm.* **2009**, *77*, 695–709, doi:10.3797/scipharm.0806-09.

17. Ochsenbein, P.; Schenk, K.J. Crystallography for Polymorphs. In *Polymorphism*; John Wiley & Sons, Ltd, 2006; pp. 139–166 ISBN 9783527607884.

18. Chattah, A.K.; Zhang, R.; Mroue, K.H.; Pfund, L.Y.; Longhi, M.R.; Ramamoorthy, A.; Garnero, C. Investigating Albendazole Desmotropes by Solid-State NMR Spectroscopy. *Mol. Pharm.* **2015**, *12*, 731–741, doi:10.1021/mp500539g.

19. Holzer, W.; Claramunt, R.M.; López, C.; Alkorta, I.; Elguero, J. A study in desmotropy. *Solid State Nucl. Magn. Reson.* **2008**, *34*, 68–76, doi:10.1016/j.ssnmr.2007.12.002.

20. Elguero, J. Polymorphism and Desmotropy in Heterocyclic Crystal Structures. *Cryst. Growth Des.* **2011**, *11*, 4731–4738, doi:10.1021/cg200970t.

21. Hilfiker, R.; Blatter, F.; Raumer, M. von Relevance of Solid-state Properties for Pharmaceutical Products. In *Polymorphism in the pharmaceutical industry*; Wiley Online Books; 2006; pp. 1–19 ISBN 9783527607884.

22. Lee, A.Y.; Erdemir, D.; Myerson, A.S. Crystal Polymorphism in Chemical Process Development. *Annu. Rev. Chem. Biomol. Eng.* **2011**, *2*, 259–280, doi:10.1146/annurev-chembioeng-061010-114224.

23. Mirmehrabi, M.; Rohani, S.; Murthy, K.S.K.; Radatus, B. Characterization of tautomeric forms

of ranitidine hydrochloride: thermal analysis, solid-state NMR, X-ray. *J. Cryst. Growth* **2004**, *260*, 517–526, doi:https://doi.org/10.1016/j.jcrysgro.2003.08.061.

24. Wojnarowska, Z.; Wlodarczyk, P.; Kaminski, K.; Grzybowska, K.; Hawelek, L.; Paluch, M. On the kinetics of tautomerism in drugs: New application of broadband dielectric spectroscopy. *J. Chem. Phys.* **2010**, *133*, 94507, doi:10.1063/1.3475688.

25. Wojnarowska, Z.; Grzybowska, K.; Hawelek, L.; Dulski, M.; Wrzalik, R.; Gruszka, I.; Paluch, M.; Pienkowska, K.; Sawicki, W.; Bujak, P.; et al. Molecular dynamics, physical stability and solubility advantage from amorphous indapamide drug. *Mol. Pharm.* **2013**, *10*, 3612–3627, doi:10.1021/mp400116q.

26. Knapik-Kowalczuk, J.; Rams-Baron, M.; Paluch, M. Current research trends in dielectric relaxation studies of amorphous pharmaceuticals: Physical stability, tautomerism, and the role of hydrogen bonding. *TrAC Trends Anal. Chem.* **2021**, *134*, 116097, doi:https://doi.org/10.1016/j.trac.2020.116097.

27. Bhatt, P.M.; Desiraju, G.R. Tautomeric polymorphism in omeprazole. *Chem. Commun.* **2007**, 2057–2059, doi:10.1039/B700506G.

28. Morris, K.R.; Griesser, U.J.; Eckhardt, C.J.; Stowell, J.G. Theoretical approaches to physical transformations of active pharmaceutical ingredients during manufacturing processes. *Adv. Drug Deliv. Rev.* **2001**, *48*, 91–114, doi:10.1016/S0169-409X(01)00100-4.

29. Hilfiker, R. *Polymorphism in the Pharmaceutical Industry*; Wiley Online Library, 2006; Vol. 308; ISBN 9783527311460.

30. Wojnarowska, Z.; Paluch, M. Tautomerism in Drug Delivery. In *Disordered Pharmaceutical Materials*; Descamps, M., Ed.; Wiley Online Library, 2016; pp. 183–200 ISBN 9783527652693.

31. Martin, Y.C. Let's not forget tautomers. *J. Comput. Aided. Mol. Des.* **2009**, *23*, 693, doi:10.1007/s10822-009-9303-2.

32. Bongioanni, A.; Bueno, M.S.; Abraham-Miranda, J.; Chattah, A.K.; Ayala, A.P.; Longhi, M.R.; Garnero, C. Investigating a Soluble Pharmaceutical Salt: Albendazole Hydrochloride. *Cryst. Growth Des.* **2019**, *19*, 4538–4545, doi:10.1021/acs.cgd.9b00348.

33. Chieng, N.; Zujovic, Z.; Bowmaker, G.; Rades, T.; Saville, D. Effect of milling conditions on the solid-state conversion of ranitidine hydrochloride form 1. *Int. J. Pharm.* **2006**, *327*, 36–44, doi:10.1016/j.ijpharm.2006.07.032.

34. Mishra, M.K.; Ramamurty, U.; Desiraju, G.R. Solid Solution Hardening of Molecular Crystals: Tautomeric Polymorphs of Omeprazole. *J. Am. Chem. Soc.* **2015**, *137*, 1794–1797, doi:10.1021/ja512817f.

35. Rams-Baron, M.; Jachowicz, R.; Boldyreva, E.; Zhou, D.; Jamroz, W.; Paluch, M. *Amorphous drugs: Benefits and challenges*; Springer, Cham, 2018; ISBN 9783319720029.

36. Nilsson Lill, S.O.; Widdifield, C.M.; Pettersen, A.; Svensk Ankarberg, A.; Lindkvist, M.; Aldred, P.; Gracin, S.; Shankland, N.; Shankland, K.; Schantz, S.; et al. Elucidating an Amorphous Form Stabilization Mechanism for Tenapanor Hydrochloride: Crystal Structure Analysis Using X-ray Diffraction, NMR Crystallography, and Molecular Modeling. *Mol. Pharm.* **2018**, *15*, 1476–1487, doi:10.1021/acs.molpharmaceut.7b01047.

37. Vogt, F.G.; Yin, H.; Forcino, R.G.; Wu, L. ^{17}O Solid-State NMR as a Sensitive Probe of Hydrogen Bonding in Crystalline and Amorphous Solid Forms of Diflunisal. *Mol. Pharm.* **2013**, *10*, 3433–3446, doi:10.1021/mp400275w.

38. Hodgkinson, P. NMR crystallography of molecular organics. *Prog. Nucl. Magn. Reson. Spectrosc.* **2020**, *118–119*, 10–53, doi:10.1016/j.pnmrs.2020.03.001.

39. Li, M.; Xu, W.; Su, Y. Solid-state NMR spectroscopy in pharmaceutical sciences. *TrAC - Trends Anal. Chem.* **2021**, *135*, 116152, doi:10.1016/j.trac.2020.116152.

40. Strachan, C.; Saarinen, J.; Lipiäinen, T.; Vuorimaa-Laukkanen, E.; Rautaniemi, K.; Laaksonen, T.; Skotnicki, M.; Dračínský, M. Spectroscopic Methods in Solid-state Characterization. In *Characterization of Pharmaceutical Nano and Microsystems*; Peltonen, L., Ed.; Wiley Online Books; Wiley Online Books, 2021; pp. 27–95 ISBN 9781119414018.

41. Sanz, J. NMR Techniques for the Study of Crystalline and Amorphous Solids BT - Defects and Disorder in Crystalline and Amorphous Solids. In; Catlow, C.R.A., Ed.; Springer Netherlands: Dordrecht, 1994; pp. 157–188 ISBN 978-94-011-1942-9.

42. Geppi, M.; Borsacchi, S.; Carignani, E. Study of Disorder by Solid-State NMR Spectroscopy. In *Disordered Pharmaceutical Materials*; Descamps, M., Ed.; Wiley Online Books; Wiley Online Library, 2016; pp. 427–466 ISBN 9783527652693.

43. Claramunt, R.M.; López, C.; Santa María, M.D.; Sanz, D.; Elguero, J. The use of NMR spectroscopy to study tautomerism. *Prog. Nucl. Magn. Reson. Spectrosc.* **2006**, *49*, 169–206, doi:10.1016/j.pnmrs.2006.07.001.

44. Wang, L.; Zhou, L.-N.; Bao, Y.; Wang, J.-K. 2-n-Butyl-3-[2′-(1H-tetrazol-5-yl)biphenyl-4-ylmethyl]-1-azonia-3-azaspiro[4.4]non-1-en-4-one bromide sesquihydrate. *Acta Crystallogr. Sect. E* **2007**, *63*, o4933–o4933, doi:https://doi.org/10.1107/S1600536807061156.

45. Bartolucci, G.; Bruni, B.; Di Vaira, M.; Giannellini, V. 2-Butyl-4-oxo-3-{[2'-(1H-tetrazol-5-yl)biphenyl-4-yl]methyl}-3-aza-1-azoniaspiro[4.4]non-1-ene chloride 1.69-hydrate (irbesartan hydrochloride 1.69-hydrate). *Acta Crystallogr. Sect. E* **2007**, *63*, o1529–o1531, doi:doi.org/10.1107/S1600536807008951.

46. Kubo, K.; Kohara, Y.; Yoshimura, Y.; Inada, Y.; Shibouta, Y.; Furukawa, Y.; Kato, T.; Nishikawa, K.; Naka, T. Nonpeptide angiotensin II receptor antagonists. Synthesis and biological activity of potential prodrugs of benzimidazole-7-carboxylic acids. *J. Med. Chem.* **1993**, *36*, 2343–2349, doi:10.1021/jm00068a011.

47. Kubo, K.; Inada, Y.; Kohara, Y.; Sugiura, Y.; Ojima, M.; Itoh, K.; Furukawa, Y.; Nishikawa, K.; Naka, T. Nonpeptide angiotensin II receptor antagonists. Synthesis and biological activity of benzimidazoles. *J. Med. Chem.* **1993**, *36*, 1772–1784, doi:10.1021/jm00064a011.

48. Heo, Y.S.; Yi, K.Y.; Yoo, S.E.; Shin, W. A non-peptide angiotensin II receptor antagonist: 2-butyl-6-methyl-5-(1-oxopyrid-2-yl)-1-{[2′-(1H-tetrazol-5-yl)biphenyl-4-yl]methyl}-1H-imidazo[5,4-b]pyridine methanol solvate. *Acta Crystallogr. Sect. C Cryst. Struct. Commun.* **1999**, *55*, 1345–1347, doi:10.1107/S0108270199004679.

49. Shin, W.; Yoon, T.-S.; Yoo, S.E. A Non-Peptide Angiotensin II Receptor Antagonist: 2-Butyl-6-dimethoxymethyl-5-phenyl-1-{[2'-(1H-tetrazol-5-yl)biphenyl-4-yl]methyl}-1H-imidazo[5,4-b]pyridine. *Acta Crystallogr. Sect. C* **1996**, *52*, 1019–1022, doi:https://doi.org/10.1107/S0108270195011978.

50. Fernández, D.; Vega, D.; Ellena, J.A. Candesartan cilexetil, an antihypertensive agent containing an extended double ester chain. *Acta Crystallogr. Sect. E Struct. Reports Online* **2005**, *61*, o309–o312, doi:10.1107/S1600536805000097.

51. Matsunaga, H.; Eguchi, T.; Nishijima, K.; Enomoto, T.; Sasaoki, K.; Nakamura, N. Solid-state characterization of candesartan cilexetil (TCV-116): Crystal structure and molecular mobility. *Chem. Pharm. Bull.* **1999**, *47*, 182–186, doi:10.1248/cpb.47.182.

52. Gao, Z.; Wu, Y.; Wu, Y.; Gong, J.; Bao, Y.; Wang, J.; Rohani, S. Self-Induced Nucleation During the Antisolvent Crystallization Process of Candesartan Cilexetil. *Cryst. Growth Des.* **2018**, *18*, 7655–7662, doi:10.1021/acs.cgd.8b01466.

53. Chi, Y.; Xu, W.; Yang, Y.; Yang, Z.; Lv, H.; Yang, S.; Lin, Z.; Li, J.; Gu, J.; Hill, C.L.; et al. Three Candesartan Salts with Enhanced Oral Bioavailability. *Cryst. Growth Des.* **2015**, *15*, 3707–3714, doi:10.1021/acs.cgd.5b00297.

54. Okazaki, T.; Suga, A.; Watanabe, T.; Kikuchi, K.; Kurihara, H.; Shibasaki, M.; Fujimori, A.; Inagaki, O.; Yanagisawa, I. Studies on nonpeptide angiotensin II receptor antagonists. II. Synthesis and biological evaluation of 5H-pyrazolo[1,5-b][1,2,4]triazole derivatives with a C-linked oxygen functional group at the 6-position. *Chem. Pharm. Bull.* **1998**, *46*, 287–293, doi:10.1248/cpb.46.287.

55. Okazaki, T.; Suga, A.; Watanabe, T.; Kikuchi, K.; Kurihara, H.; Shibasaki, M.; Fujimori, A.; Inagaki, O.; Yanagisawa, I. Studies on nonpeptide angiotensin II receptor antagonists. I. Synthesis and biological evaluation of pyrazolo [1,5-b][1,2,4]triazole derivatives with alkyl substituents. *Chem. Pharm. Bull.* **1998**, *46*, 69–78, doi:10.1248/cpb.46.69.

56. Bradbury, R.H.; Allott, C.P.; Dennis, M.; Girdwood, J.A.; Kenny, P.W.; Major, J.S.; Oldham, A.A.; Ratcliffe, A.H.; Rivett, J.E. New nonpeptide angiotensin II receptor antagonists. 3. Synthesis, biological properties, and structure-activity relationships of 2-alkyl-4-(biphenylylmethoxy)pyridine derivatives. *J. Med. Chem.* **1993**, *36*, 1245–1254, doi:10.1021/jm00061a016.

57. Okazaki, T.; Watanabe, T.; Kikuchi, K.; Suga, A.; Shibasaki, M.; Fujimori, A.; Inagaki, O.; Yanagisawa, I. Studies on nonpeptide angiotensin II receptor antagonists. IV. Synthesis and biological evaluation of 4-acrylamide-1H-imidazole derivatives. *Chem. Pharm. Bull.* **1998**, *46*, 973–981, doi:10.1248/cpb.46.973.

58. Tan, N.P.H.; Taylor, M.K.; Bottle, S.E.; Wright, C.E.; Ziogas, J.; White, J.M.; Schiesser, C.H.; Jani, N. V Novel paramagnetic AT_1 receptor antagonists. *Chem. Commun.* **2011**, *47*, 12083–12085, doi:10.1039/C1CC14920B.

59. Tessler, L.; Goldberg, I. Losartan, an antihypertensive drug. *Acta Crystallogr. Sect. E* **2004**, *60*, o1830--o1832, doi:10.1107/S1600536804022949.

60. Yanagisawa, H.; Amemiya, Y.; Kanazaki, T.; Shimoji, Y.; Fujimoto, K.; Kitahara, Y.; Sada, T.; Mizuno, M.; Ikeda, M.; Miyamoto, S.; et al. Nonpeptide Angiotensin II Receptor Antagonists: Synthesis, Biological Activities, and Structure−Activity Relationships of Imidazole-5-carboxylic Acids Bearing Alkyl, Alkenyl, and Hydroxyalkyl Substituents at the 4-Position and Their Related Compounds. *J. Med. Chem.* **1996**, *39*, 323–338, doi:10.1021/jm950450f.

61. Betz, R.; Hosten, E.; Gerber, T.; Dayananda, A.S.; Yathirajan, H.S.; Saji, T. Redetermination of the structure of olmesartan medoxomil, (5-methyl-2- oxo-2H-1,3-dioxol-4-yl)-methyl-4-(2-hydroxypropan-2-yl)-2-propyl-1-(-[2- (2H-1,2,3,4-tetrazol-5-yl)-phenyl]phenylmethyl)-1H-imidazole-5- carboxylate, C29H30N6O6. *Zeitschrift für Krist. - New Cryst. Struct.* **2013**, *228*, 141–143, doi:doi:10.1524/ncrs.2013.0073.

62. Ishii, H.; Yamaguchi, K.; Seki, H.; Sakamoto, S.; Tozuka, Y.; Oguchi, T.; Yamamoto, K. Crystal Structure of the Alcoholates and the Ansolvate of PNU-97018, an Angiotensin II Receptor Antagonist. *Chem. Pharm. Bull.* **2002**, *50*, 1022–1027, doi:10.1248/cpb.50.1022.

63. Cappelli, A.; Nannicini, C.; Gallelli, A.; Giuliani, G.; Valenti, S.; Mohr, G. l. P.; Anzini, M.; Mennuni, L.; Ferrari, F.; Caselli, G.; et al. Design, Synthesis, and Biological Evaluation of AT1 Angiotensin II Receptor Antagonists Based on the Pyrazolo[3,4-b]pyridine and Related Heteroaromatic Bicyclic Systems. *J. Med. Chem.* **2008**, *51*, 2137–2146, doi:10.1021/jm7011563.

64. Ellingboe, J.W.; Antane, M.; Nguyen, T.T.; Collini, M.D.; Antane, S.; Bender, R.; Hartupee, D.; White, V.; McCallum, J. Pyrido[2,3-d]pyrimidine Angiotensin II Antagonists. *J. Med. Chem.* **1994**, *37*, 542–550, doi:10.1021/jm00030a013.

65. Wang, J.-R.; Wang, X.; Lu, L.; Mei, X. Highly Crystalline Forms of Valsartan with Superior Physicochemical Stability. *Cryst. Growth Des.* **2013**, *13*, 3261–3269, doi:10.1021/cg400762w.

66. Skotnicki, M.; Apperley, D.C.; Aguilar, J.A.; Milanowski, B.; Pyda, M.; Hodgkinson, P. Characterization of Two Distinct Amorphous Forms of Valsartan by Solid-State NMR. *Mol. Pharm.* **2016**, *13*, 211–222, doi:10.1021/acs.molpharmaceut.5b00646.

67. Fung, B.M.; Khitrin, A.K.; Ermolaev, K. An improved broadband decoupling sequence for liquid crystals and solids. *J. Magn. Reson.* **2000**, *142*, 97–101, doi:https://doi.org/10.1006/jmre.1999.1896.

68. Mildner, T.; Ernst, H.; Freude, D. ^{207}Pb NMR detection of spinning-induced temperature gradients in MAS rotors. *Solid State Nucl. Magn. Reson.* **1995**, *5*, 269–271, doi:10.1016/0926-2040(95)01189-1.

69. Apperley, D.; Harris, R.; Hodgkinson, P. *Solid-State NMR: Basic Principles & Practice*; Momentum Press: New York, 2012; ISBN 9781606503522.

70. Gervais, C.; Babonneau, F.; Maquet, J.; Bonhomme, C.; Massiot, D.; Framery, E.; Vaultier, M. ^{15}N cross-polarization using the inversion-recovery cross-polarization technique and ^{11}B magic angle spinning NMR studies of reference compounds containing B - N bonds. *Magn. Reson. Chem.* **1998**, *36*, 407–414, doi:10.1002/(sici)1097-458x(199806)36:6<407::aid-omr295>3.3.co;2-p.

71. Zorin V. Gsim – a visualisation and processing program for solid-state NMR Available online: https://sourceforge.net/projects/gsim/ (accessed on Dec 1, 2020).

72. Ni, Q.Z.; Markhasin, E.; Can, T. V.; Corzilius, B.; Tan, K.O.; Barnes, A.B.; Daviso, E.; Su, Y.; Herzfeld, J.; Griffin, R.G. Peptide and Protein Dynamics and Low-Temperature/DNP Magic Angle Spinning NMR. *J. Phys. Chem. B* **2017**, *121*, 4997–5006, doi:10.1021/acs.jpcb.7b02066.

73. Raghavan, K.; Dwivedi, A.; Campbell, G.C.; Johnston, E.; Levorse, D.; McCauley, J.; Hussain, M. A Spectroscopic Investigation of Losartan Polymorphs. *Pharm. Res.* **1993**, *10*, 900–904, doi:10.1023/A:1018973530443.

74. Skotnicki, M.; Jadach, B.; Skotnicka, A.; Milanowski, B.; Tajber, L.; Pyda, M.; Kujawski, J. Physicochemical characterization of a co-amorphous atorvastatin-irbesartan system with a potential application in fixed-dose combination therapy. *Pharmaceutics* **2021**, *13*, 1–20, doi:10.3390/pharmaceutics13010118.

75. Kolehmainen, E.; Ośmiałowski, B. ^{15}N NMR Studies of tautomerism. *Int. Rev. Phys. Chem.* **2012**, *31*, 567–629, doi:10.1080/0144235X.2012.734157.

76. Veinberg, S.L.; Johnston, K.E.; Jaroszewicz, M.J.; Kispal, B.M.; Mireault, C.R.; Kobayashi, T.; Pruski, M.; Schurko, R.W. Natural abundance ^{14}N and ^{15}N solid-state NMR of pharmaceuticals and their polymorphs. *Phys. Chem. Chem. Phys.* **2016**, *18*, 17713–17730, doi:10.1039/C6CP02855A.

77. Brownbill, N.J.; Sprick, R.S.; Bonillo, B.; Pawsey, S.; Aussenac, F.; Fielding, A.J.; Cooper, A.I.; Blanc, F. Structural Elucidation of Amorphous Photocatalytic Polymers from Dynamic Nuclear Polarization Enhanced Solid State NMR. *Macromolecules* **2018**, *51*, 3088–3096, doi:10.1021/acs.macromol.7b02544.

78. Smith, A.N.; Märker, K.; Hediger, S.; De Paëpe, G. Natural Isotopic Abundance ^{13}C and ^{15}N

Multidimensional Solid-State NMR Enabled by Dynamic Nuclear Polarization. *J. Phys. Chem. Lett.* **2019**, *10*, 4652–4662, doi:10.1021/acs.jpclett.8b03874.

79. Lilly Thankamony, A.S.; Wittmann, J.J.; Kaushik, M.; Corzilius, B. Dynamic nuclear polarization for sensitivity enhancement in modern solid-state NMR. *Prog. Nucl. Magn. Reson. Spectrosc.* **2017**, *102–103*, 120–195, doi:10.1016/j.pnmrs.2017.06.002.

80. Fischer, D.; Klapötke, T.M.; Reymann, M.; Schmid, P.C.; Stierstorfer, J.; Sućeska, M. Synthesis of 5-(1H-Tetrazolyl)-1-hydroxy-tetrazole and Energetically Relevant Nitrogen-Rich Ionic Derivatives. *Propellants, Explos. Pyrotech.* **2014**, *39*, 550–557, doi:https://doi.org/10.1002/prep.201300152.

81. Goddard, R.; Heinemann, O.; Kruger, C. α-1H-1,2,3,4-Tetrazole. *Acta Crystallogr. Sect. C* **1997**, *53*, 590–592, doi:https://doi.org/10.1107/S0108270197000772.

82. Araujo-Andrade, C.; Reva, I.; Fausto, R. Tetrazole acetic acid: Tautomers, conformers, and isomerization. *J. Chem. Phys.* **2014**, *140*, doi:10.1063/1.4864119.

83. Tong, S.-W.; Song, W.-D.; Li, S.-J.; Miao, D.-L.; An, J.-B. 5-[4-(1H-Imidazol-1-yl)phen-yl]-1H-tetra-zole. *Acta Crystallogr. Sect. E* **2012**, *68*, o1274, doi:10.1107/S1600536812013670.

84. Steel, P.J. Heterocyclic tautomerism. XI. Structures of 5,5′-bitetrazole and 1-methyl-5-(2′-pyridyl)tetrazole at 130 K. *J. Chem. Crystallogr.* **1996**, *26*, 399–402, doi:10.1007/BF01665818.

85. Rizk, A.T.; Kilner, C.A.; Halcrow, M.A. Two regioisomers of (pyrid-2-yl)tetrazole which form two-dimensional five- and six-connected nets through hydrogen bonding. *CrystEngComm* **2005**, *7*, 359–362, doi:10.1039/B506015J.

86. Fischer, N.; Izsák, D.; Klapötke, T.M.; Stierstorfer, J. The Chemistry of 5-(Tetrazol-1-yl)-2H-tetrazole: An Extensive Study of Structural and Energetic Properties. *Chem. – A Eur. J.* **2013**, *19*, 8948–8957, doi:https://doi.org/10.1002/chem.201300691.

87. Butler, R.N.; Garvin, V.C.; Lumbroso, H.; Liégeois, C. A substituent correlation and medium effects on the annular tautomerism of substituted 5-aryltetrazoles: the nitrogen analogues of benzoic acids. A carbon-13 n.m.r. and dipole moment study. *J. Chem. Soc. Perkin Trans. 2* **1984**, 721–725, doi:10.1039/P29840000721.

88. Mazurek, A.P.; Sadlej-Sosnowska, N. Studies on tautomerism in tetrazole: comparison of Hartree–Fock and density functional theory quantum chemical methods. *Chem. Phys. Lett.* **2000**, *330*, 212–218, doi:https://doi.org/10.1016/S0009-2614(00)01060-5.

89. Zhaoxu, C.; Heming, X. Ab initio study of thermodynamic and kinetic properties of tetrazole and its tautomerization. *J. Mol. Struct. THEOCHEM* **1998**, *453*, 65–70, doi:10.1016/S0166-1280(98)00177-8.

90. Wong, M.W.; Leung-Toung, R.; Wentrup, C. Tautomeric equilibrium and hydrogen shifts of tetrazole in the gas phase and in solution. *J. Am. Chem. Soc.* **1993**, *115*, 2465–2472, doi:10.1021/ja00059a048.

91. Araya-Sibaja, A.M.; Urgellés, M.; Vásquez-Castro, F.; Vargas-Huertas, F.; Vega-Baudrit, J.R.; Guillén-Girón, T.; Navarro-Hoyos, M.; Cuffini, S.L. The effect of solution environment and the electrostatic factor on the crystallisation of desmotropes of irbesartan. *RSC Adv.* **2019**, *9*, 5244–5250, doi:10.1039/c8ra10146a.

92. Carignani, E.; Borsacchi, S.; Geppi, M. Detailed characterization of the dynamics of ibuprofen in the solid state by a multi-technique NMR approach. *ChemPhysChem* **2011**, *12*, 974–981, doi:10.1002/cphc.201000946.